Comparison of Reluctance and Surface Permanent Magnet Coaxial Magnetic Gears

Shima Hasanpour
Dept. of Elec. And Comp. Engr.
Texas A&M University
College Station, Texas 77843
shimahasanpour@tamu.edu

Matthew C. Gardner
Dept. of Elec. And Comp. Engr.
Texas A&M University
College Station, Texas 77843
gardner1100@tamu.edu

Matthew Johnson
Army Research Lab
U. S. Army CCDC
College Station, TX, USA
matthew.c.johnson186.civ@mail.mil

Hamid A. Toliyat
Dept. of Elec. And Comp. Engr.
Texas A&M University
College Station, Texas 77843
toliyat@tamu.edu

***Abstract*—The noncontact operation of magnetic gears offers significant potential advantages over mechanical gears. Reluctance magnetic gears (RMGs) have been proposed as an alternative to surface permanent magnet gears (SPMGs) at high speeds. This paper explains the operating principles of RMGs and provides a thorough parametric comparison between RMGs and SPMGs using 2-D and 3-D finite element analysis (FEA). SPMGs are found to outperform RMGs in torque density, as expected. However, contrary to the results of nonoptimized comparisons in previous papers, optimal SPMGs also can achieve better magnet utilizations and efficiencies than optimal RMGs. Additionally, the RMGs with the highest torque densities suffer from significantly more torque ripple than the SPMGs with the highest torque densities. Also, the simulations demonstrate that the optimal SPMGs and optimal RMGs with the same stack lengths tend to suffer comparable reductions in torque from end effects.**

***Keywords*—End effects, finite-element analysis (FEA), magnet utilization, magnetic gear, optimization, permanent magnet, reluctance magnetic gear, torque density, torque ripple.**

I. Introduction

Magnetic gears are an interesting alternative to mechanical gears for converting energy between low-torque, high-speed rotation and high-torque, low-speed rotation. However, unlike mechanical gears, magnetic gears operate without employing contact between the rotors. A magnetic gear uses the interaction between modulated magnetic fields, instead of using interlocking mechanical teeth. This contactless operation provides potential benefits, such as improved reliability, reduced acoustic noise, and reduced maintenance requirements (no lubrication oil). Therefore, magnetic gears have been proposed for various applications, including traction [1], propulsion [2], and wind [3] and wave energy [4].

The most widely studied magnetic gear topology is the radial flux coaxial surface permanent magnet gear (SPMG) shown in Fig. 1(a) [1]-[3], [5]. This topology includes three rotors: the inner low pole count, high-speed permanent magnet (PM) rotor (Rotor 1), the intermediate rotor consisting of ferromagnetic pieces (modulators) separated by nonmagnetic slots (Rotor 2), and the outer high pole count, low-speed PM rotor (Rotor 3).

Much of the existing magnetic gear literature focuses on low-speed, high-torque applications [3], [4], [6]; however, magnetic gears have also been proposed for higher speed applications [7]. Unfortunately, higher speed operation presents some electromagnetic and mechanical challenges for the conventional SPMG. Electromagnetically, higher speed rotation leads to higher frequency variation of the magnetic fields and higher eddy current losses, especially in the PMs. This issue can be mitigated by axially segmenting the magnets [8], which is analogous to laminating motor cores. However, this increases the manufacturing complexity. High-speed operation also makes retaining the Rotor 1 PMs more challenging. A sleeve around the PMs can hold them in place, but this increases the effective air gap, which reduces the design's torque, and can incur eddy current losses if the sleeve is electrically conductive [9]. Alternatively, the PMs could be embedded in the Rotor 1 laminations to form an interior PM (IPM) rotor. However, thin bridges in laminations often provide flux leakage paths, which reduce the air gap flux produced by the PMs [10]. Additionally, these thin bridges can experience large mechanical stresses at high speeds [10].

Another magnetic gear alternative for high-speed applications is the reluctance magnetic gear (RMG), which is illustrated in Fig. 1(b) [11]-[15]. The RMG replaces the Rotor 1 PMs with teeth, such that Rotor 1 can be formed from a single stack of laminations, as shown in Fig. 1(b). Eliminating the Rotor 1 PMs simplifies the mechanical challenges associated with rotating Rotor 1 at high speeds and removes the Rotor 1 PM eddy current losses. Flux switching magnetic gears have also been proposed for high-speed applications [14]. Flux switching magnetic gears are similar to RMGs but contain extra PMs in the spaces between the modulators, which increases the manufacturing complexity. However, this study solely compares SPMGs and RMGs. While previous papers have proposed RMGs and evaluated a few designs [11]-[14], this paper uses significant 2-D and 3-D parametric sweeps to

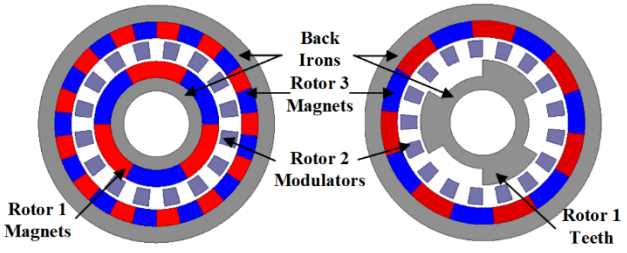

Fig. 1. Cross-sections of (a) an SPMG and (b) an RMG.

characterize the capabilities of RMGs and compare optimal RMGs against optimal SPMGs. This paper also provides a more accurate description of RMGs' operating principles.

II. Operating Principles

The principle of operation in coaxial magnetic gears is to modulate the magnetomotive force (MMF) of magnets through the modulators and create a flux distribution in the air gap [16]. In SPMGs, there are two sets of magnets, each creating its own MMF with its specific frequency. However, there is only one set of magnets in RMGs that can create the MMF, which will be modulated once by the permeance distribution of Rotor 2 and once by the permeance distribution of the Rotor 1 teeth.

The operating principles of RMGs are similar to those of SPMGs. However, there are a few key differences. First, instead of the MMF distribution developed by the Rotor 1 PMs in an SPM gear, the Rotor 1 teeth in an RMG produce a permeance distribution. Equations (1) – (3) provide the Rotor 1 permeance ($\mathcal{P}_1$), Rotor 2 permeance ($\mathcal{P}_2$), and Rotor 3 MMF ($\mathcal{F}_3$) functions of an RMG with N_1 teeth on Rotor 1, Q_2 modulators on Rotor 2, and P_3 pole pairs on Rotor 3. In these equations, $\mathcal{P}_{1,0}$ and $\mathcal{P}_{2,0}$ represent the constant permeance components, $\mathcal{P}_{1,i}$, $\mathcal{P}_{2,j}$, and $\mathcal{F}_{3,k}$ represent the permeance and MMF spatial harmonic coefficients, and θ_1, θ_2, and θ_3 represent the instantaneous positions of Rotors 1, 2, and 3 at time t, which are given by (4), (5), and (6), respectively. In (4), (5), and (6), ω_1, ω_2, and ω_3 represent the speeds of the three rotors, and $\theta_{1,0}$, $\theta_{2,0}$, and $\theta_{3,0}$ represent the initial positions of the rotors.

$$\mathcal{P}_1(\theta) = \mathcal{P}_{1,0} + \sum_{i=1}^{\infty} \mathcal{P}_{1,i} \cos\big(iN_1(\theta - \theta_1)\big) \tag{1}$$

$$\mathcal{P}_2(\theta) = \mathcal{P}_{2,0} + \sum_{j=1}^{\infty} \mathcal{P}_{2,j} \cos\big(jQ_2(\theta - \theta_2)\big) \tag{2}$$

$$\mathcal{F}_3(\theta) = \sum_{k=1}^{\infty} \mathcal{F}_{3,k} \cos\big(kP_3(\theta - \theta_3)\big) \tag{3}$$

$$\theta_1 = \omega_1 t + \theta_{1,0} \tag{4}$$

$$\theta_2 = \omega_2 t + \theta_{2,0} \tag{5}$$

$$\theta_3 = \omega_3 t + \theta_{3,0} \tag{6}$$

The Rotor 3 PMs' MMF is modulated by the Rotor 2 modulators to produce the flux distribution given by (7), where $\Phi_{2,3,0,k}$ represents the flux spatial harmonics produced by the interaction of $\mathcal{P}_{2,0}$ and $\mathcal{F}_{3,k}$ and $\Phi_{2,3,j,k}$ represents the flux spatial harmonics produced by the interaction of $\mathcal{P}_{2,j}$ and $\mathcal{F}_{3,k}$, as defined in (8) and (9). Similarly, the modulation of the Rotor 3 MMF by the Rotor 1 teeth produces the flux distribution given by (10), where $\Phi_{1,3,0,k}$ represents the set of flux spatial harmonics produced by the interaction of $\mathcal{P}_{1,0}$ and $\mathcal{F}_{3,k}$ and $\Phi_{1,3,i,k}$ is the set of flux spatial harmonics produced by the interaction of $\mathcal{P}_{1,i}$ and $\mathcal{F}_{3,k}$, as defined in (11) and (12).

The gearing action can be achieved by matching the pole counts and speeds of a term from (9) with a term from (12). This yields the relationship between N_1, Q_2, and P_3 given by (13), where k_a and k_b are odd integers, and i and j are integers and can be positive, 0, or negative. Then, the speed relationship is given by (14). Selecting $k_a = 1$, $k_b = 1$, $j = -1$, and $i = 1$ yields (15) and (16). Then, the gear ratio (G) is given by (17) if Rotor 2 is stationary, with the negative sign denoting that Rotors 1 and 3 rotate in opposite directions, or by (18) if Rotor 3 is stationary. For this study, Rotor 2 is held stationary and Rotor 3 is used as the low speed rotor, with the gear ratio given by (17).

$$|k_a P_3 + jQ_2| = |k_b P_3 + iN_1| \tag{13}$$

$$\frac{k_a P_3 \omega_3 + jQ_2\omega_2}{k_a P_3 + jQ_2} = \frac{k_b P_3 \omega_3 + iN_1\omega_1}{k_b P_3 + iN_1} \tag{14}$$

$$Q_2 = N_1 + 2P_3 \tag{15}$$

$$Q_2\omega_2 = N_1\omega_1 + 2P_3\omega_3 \tag{16}$$

$$G\big|_{\omega_{2=0}} = \frac{\omega_1}{\omega_3} = -\frac{2P_3}{N_1} \tag{17}$$

$$G\big|_{\omega_{3=0}} = \frac{\omega_1}{\omega_2} = \frac{Q_2}{N_1} \tag{18}$$

The gear ratio in previous papers [11]-[15] was derived by multiplying the permeance of Rotor 1 by the permeance of Rotor 2 and by the MMF of Rotor 3 ($\mathcal{P}_1\mathcal{P}_2\mathcal{F}_3$) which cannot be physically correct because the multiplication of two permeances and an MMF has no physical meaning, although

$$\Phi_{2,3}(\theta) = \mathcal{F}_3(\theta)\mathcal{P}_2(\theta) = \sum_{k=1}^{\infty} \Phi_{2,3,0,k}(\theta) + \sum_{j=1}^{\infty}\sum_{k=1}^{\infty} \Phi_{2,3,j,k}(\theta) \tag{7}$$

$$\Phi_{2,3,0,k}(\theta) = \mathcal{F}_{3,k}\mathcal{P}_{2,0} \cos\big(kP_3(\theta - \theta_3)\big) \tag{8}$$

$$\Phi_{2,3,j,k}(\theta) = \frac{\mathcal{F}_{3,k}\mathcal{P}_{2,j}}{2}\left(\cos\left((kP_3 + jQ_2)\left(\theta - \frac{kP_3\theta_3 + jQ_2\theta_2}{kP_3 + jQ_2}\right)\right) + \cos\left((kP_3 - jQ_2)\left(\theta - \frac{kP_3\theta_3 - jQ_2\theta_2}{kP_3 - jQ_2}\right)\right)\right) \tag{9}$$

$$\Phi_{1,3}(\theta) = \mathcal{F}_3(\theta)\mathcal{P}_1(\theta) = \sum_{k=1}^{\infty} \Phi_{1,3,0,k}(\theta) + \sum_{i=1}^{\infty}\sum_{k=1}^{\infty} \Phi_{1,3,i,k}(\theta) \tag{10}$$

$$\Phi_{1,3,0,k}(\theta) = \mathcal{F}_{3,k}\mathcal{P}_{1,0} \cos\big(kP_3(\theta - \theta_3)\big) \tag{11}$$

$$\Phi_{1,3,i,k}(\theta) = \frac{\mathcal{F}_{3,k}\mathcal{P}_{1,i}}{2}\left(\cos\left((kP_3 + iN_1)\left(\theta - \frac{kP_3\theta_3 + iN_1\theta_1}{kP_3 + iN_1}\right)\right) + \cos\left((kP_3 - iN_1)\left(\theta - \frac{kP_3\theta_3 - iN_1\theta_1}{kP_3 - iN_1}\right)\right)\right) \tag{12}$$

the same gear ratio is ultimately obtained. Instead, the operation of the gear is based on coupling a flux harmonic created by the modulation of the Rotor 3 PMs by the Rotor 2 modulators, as defined in (9), to a flux harmonic created by the modulation of the Rotor 3 PMs by the Rotor 1 teeth, as defined in (12). In order to illustrate this operating principle, a sample RMG with N_1 = 4, Q_2 = 22, and P_3 = 9 was simulated and the results are shown in Fig. 2. Two scenarios were evaluated: the scenario with Rotor 1 and Rotor 3 present without the Rotor 2 modulators and the scenario with Rotor 2 and Rotor 3 present without the Rotor 1 teeth. Fig. 2(a) shows the inner air gap radial flux densities obtained for these two scenarios, and Fig. 2(b) shows the normalized FFT of the inner air gap radial flux densities. Both scenarios produce a large 9th harmonic component corresponding to P_3 and a 13th harmonic component corresponding to $|P_3 - Q_2|$ or $|P_3 + N_1|$. In this case, it is the interaction of these 13th harmonic components that produces the gearing behavior. Fig. 2(c) illustrates the flux lines for the scenario without the Rotor 2 modulators. Fig. 2(d) illustrates the flux lines for the scenario without the Rotor 1 teeth.

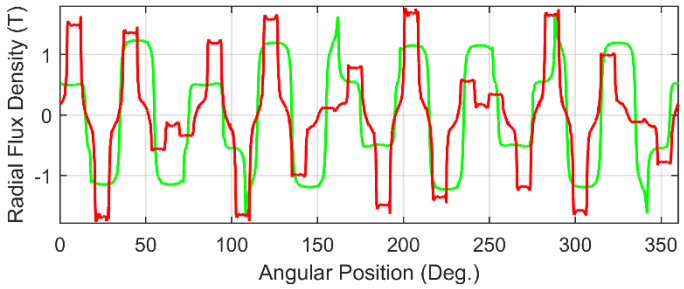

(a)

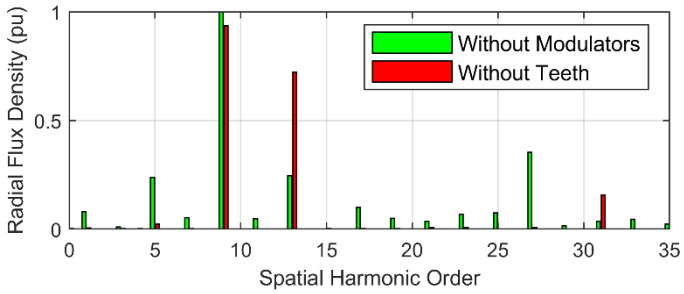

(b)

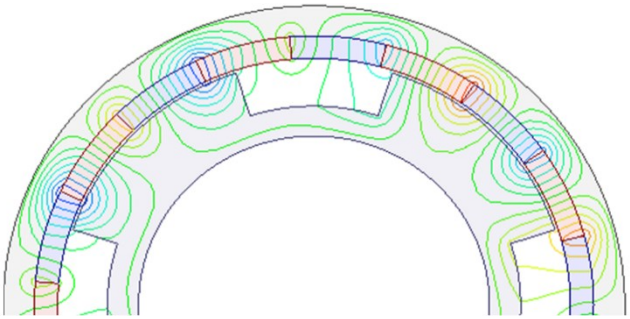
(c)

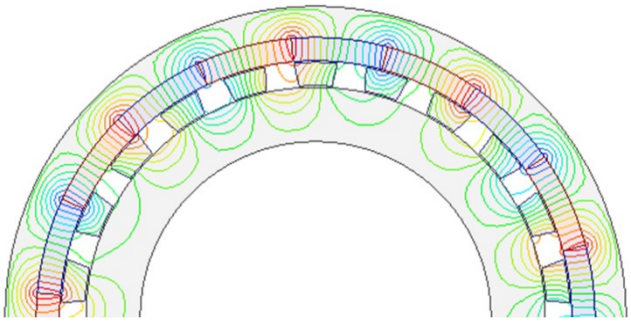
(d)

Fig. 2. (a) Distribution of radial flux density in the inner air gap, (b) normalized FFT of the radial flux density in the inner air gap, and flux lines for (c) a structure with no modulators and (d) a structure with no Rotor 1 teeth.

III. Design Study Methodology

Both the SPMG and the RMG topologies were evaluated using 2-D finite element analysis (FEA) simulations at the slip torque alignment. The ferromagnetic components (back irons, Rotor 1 teeth, and modulators) are made of M47 steel (26 gauge), and NdFeB N42 is used for the magnets. Table I shows the design parameter values evaluated for each topology. Table II summarizes the values considered for the RMG tooth count and the SPMG Rotor 1 pole pair count for each G_{Int} value without including unnecessary suboptimal cases with high pole counts and high gear ratios. Reference [15] optimizes the shape and skew of the RMG teeth to reduce torque ripple; however, this study only evaluates arc-shaped modulators and magnets, as the alterations in [15] do not significantly increase the designs' slip torques. The different torque densities evaluated in this study are volumetric torque density (VTD), the Rotor 3 slip torque divided by the gear's total active volume, gravimetric torque density (GTD), the Rotor 3 slip torque divided the gear's total active mass, and PM GTD, the Rotor 3 slip torque divided by the gear's total PM mass.

After all designs specified in Tables I and II were evaluated using magnetostatic 2-D FEA, the optimal designs were evaluated using magnetostatic 3-D FEA at the stack lengths

TABLE I. Design Parameter Sweep Ranges

Name	Description	Values
G_{Int}	Integer part of the gear ratio	4, 6, 10, 16
R_{Out}	Outer radius (mm)	100
T_{BI1}	Rotor 1 back iron thickness (mm)	5, 10, 20
T_{BI3}	Rotor 3 back iron thickness (mm)	5, 10, 20
T_{Mods}	Modulators thickness (mm)	5, 10, 20
T_{PM1}	SPMG Rotor 1 PM thickness (mm)	3, 6, 9, 12, 15
k_{PM}	SPMG PM thickness ratio	0.5, 0.75, 1
T_{TH}	RMG Rotor 1 teeth thickness (mm)	3, 6, 9, 12, 15
T_{PM3}	RMG Rotor 3 PM thickness (mm)	3, 6, 9, 12, 15
α_{TH}	RG teeth tangential fill factor	0.35, 0.4, … 0.55
α_{Mods}	Modulator tangential fill factor	0.5
α_{PM}	PM tangential fill factor	1
T_{AG}	Air gap thickness (mm)	0.5
L_{Stack}	Stack length (mm)	20, 30, 50, 70

TABLE II. Rotor 1 Tooth Count for RMG (N_1) and Pole Pair Count for SPMG (P_1) Sweep Ranges

G_{Int}	RMG	SPMG
4	3, 4, … 10	3, 4, … 18
6	3, 4, … 7	3, 4, … 13
10	3, 4, 5, 6	3, 4, … 9
16	3, 4, 5	3, 4, 5, 6

specified in Table I to investigate the end effect impacts on the torque. Additionally, 2-D transient FEA was used to evaluate the electromagnetic efficiencies of the optimal designs.

The gear ratio for both topologies is defined as the ratio of the Rotor 1 speed to the Rotor 3 speed with the modulators fixed, so (17) gives the gear ratio for RMGs. For SPMGs, (19) gives the gear ratio (G_{SPMG}), where $P_{3,SPMG}$ is the SPMG's Rotor 3 pole pair count. The number of modulators is given by (15) for RMGs, and (20) gives the modulator count ($Q_{2,SPMG}$) for SPMGs.

$$G_{SPMG}\big|_{\omega_{2=0}} = \frac{\omega_1}{\omega_3} = -\frac{P_{3,SPMG}}{P_1} \tag{19}$$

$$Q_{2,SPMG} = P_1 + P_{3,SPMG} \tag{20}$$

The Rotor 3 PM pole pair counts are derived from the parameters in Table I using (21) for SPMGs and (22) for RMGs to avoid integer gear ratios, which tend to result in designs with large torque ripple [3], [17], [18]. Substituting the $P_{3,SPMG}$ of equation (21) into (20) gives an even number of modulators for any combination of P_1 and G_{Int}, which ensures that the design has some symmetry. This symmetry cancels out unbalanced magnetic forces on the rotors. However, based on (22) and (15), an RMG design will only have symmetry if N_1 is even.

$$P_{3,SPMG} = \begin{cases} G_{Int}P_1 + 1 & \text{for } (G_{Int}+1)P_1 \text{ odd} \\ G_{Int}P_1 + 2 & \text{for } (G_{Int}+1)P_1 \text{ even} \end{cases} \tag{21}$$

$$P_3 = \begin{cases} 0.5(G_{Int}N_1 + 1) & \text{for } G_{Int}N_1 \text{ odd} \\ 0.5(G_{Int}N_1 + 2) & \text{for } G_{Int}N_1 \text{ even} \end{cases} \tag{22}$$

The PM thickness ratio (k_{PM}) relates the thickness of the magnets on Rotor 3 (T_{PM3}) to the thickness of the magnets on Rotor 1, (T_{PM1}) for SPMGs according to (23). Rotor 1 has fewer poles than Rotor 3, so the optimal designs have thicker magnets on Rotor 1 [17], [19]; however, if the Rotor 1 magnets are too much thicker than the Rotor 3 magnets, then the Rotor 3 magnets may be demagnetized. Thus, k_{PM} is varied between 0.5 and 1.

$$T_{PM3} = k_{PM}T_{PM1} \tag{23}$$

IV. Results

Fig.3 illustrates that SPMGs outperform RMGs in terms of VTD, GTD, and PM GTD. While the RMG is expected to achieve lower VTD and GTD than the SPMG, the reduced PM GTD contradicts the assertions of a previous paper [20]. Even though the RMG has no PMs on Rotor 1, the associated reduction in torque outweighs the reduction in PM mass, so RMGs actually use PM material less effectively than SPMGs. Thus, a RGM can require at least 3 times as much PM material to get the same torque as an SPMG design based on Fig. 3(c).

Fig. 4 shows that, similarly to SPMG designs, RMG designs with larger gear ratios are optimized with fewer Rotor 1 teeth. However, for a given gear ratio, the optimal RMG Rotor 1 teeth count is much lower than the optimal SPMG Rotor 1 pole pair count, which means that the optimal Rotor 3 pole pair and Rotor 2 modulator counts for a given gear ratio will also be lower for an RMG than for an SPMG. For an SPMG, increasing the gear

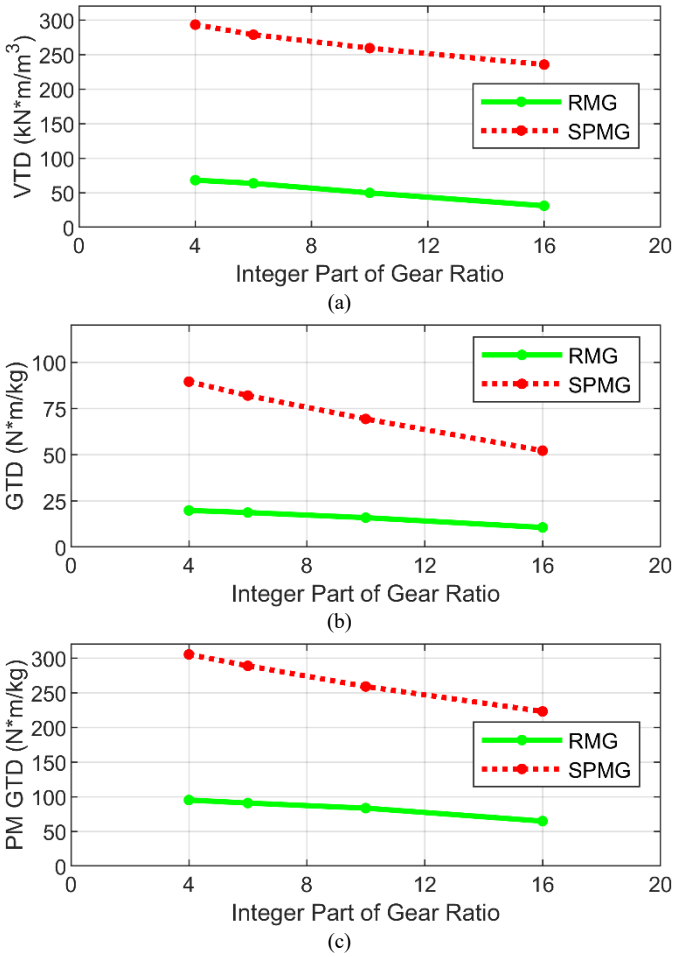

Fig. 3. Impact of G_{Int} on the achievable (a) VTD, (b) GTD, and (c) PM GTD for RMGs and SPMGs based on 2-D simulations.

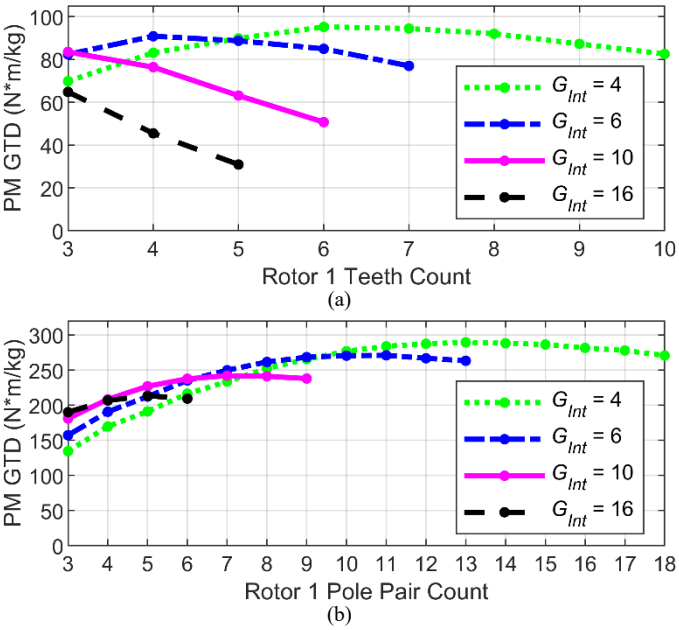

Fig. 4. Impact of (a) RMG Rotor 1 teeth count and (b) SPMG Rotor 1 pole pair count on the achievable PM GTD of designs with G_{Int} based on 2-D simulations.

ratio tends to reduce the optimal P_1 and increase the optimal $P_{3,SPMG}$, resulting in PM pole counts that are farther from the optimal values that would be selected for a similar design with a 1:1 gear ratio. However, the RMG has only one set of magnets to be optimized for any certain gear ratio, avoiding the conflict between the optimal values of P_1 and $P_{3,SPMG}$ that reduces the torque densities of SPMGs with higher gear ratio. Therefore, the optimal P_3 value for an RMG can be maintained by reducing N_1 as the gear ratio increases. However, reducing N_1 to a value of 1 or 2 results in an integer gear ratio, which can produce excessive torque ripples [3], so these designs were not simulated, even though they might produce the optimal PM GTDs for RMGs with larger gear ratios at this outer radius.

A previous paper suggested that the elimination of the PM eddy currents from Rotor 1 may make an RMG more efficient than an SPMG [11]. This is not generally accurate, as demonstrated by Fig. 5, which illustrates the Pareto optimal fronts of the RMGs and SPMGs that maximize full load electromagnetic efficiency and PM GTD with Rotor 3 speeds of 100, 1000, and 5000 rpm. At each speed, the optimal SPMG designs are significantly more efficient than the optimal RMG designs. Of course, the losses in either type of gear could be reduced by segmenting the PMs or by using a less lossy grade of steel. These changes might affect RMGs and SPMGs differently, due to different loss distributions. Nonetheless, the RMG's efficiency is limited by the fact that it requires significantly more steel and PM material to achieve the same torque as an optimal SPMG.

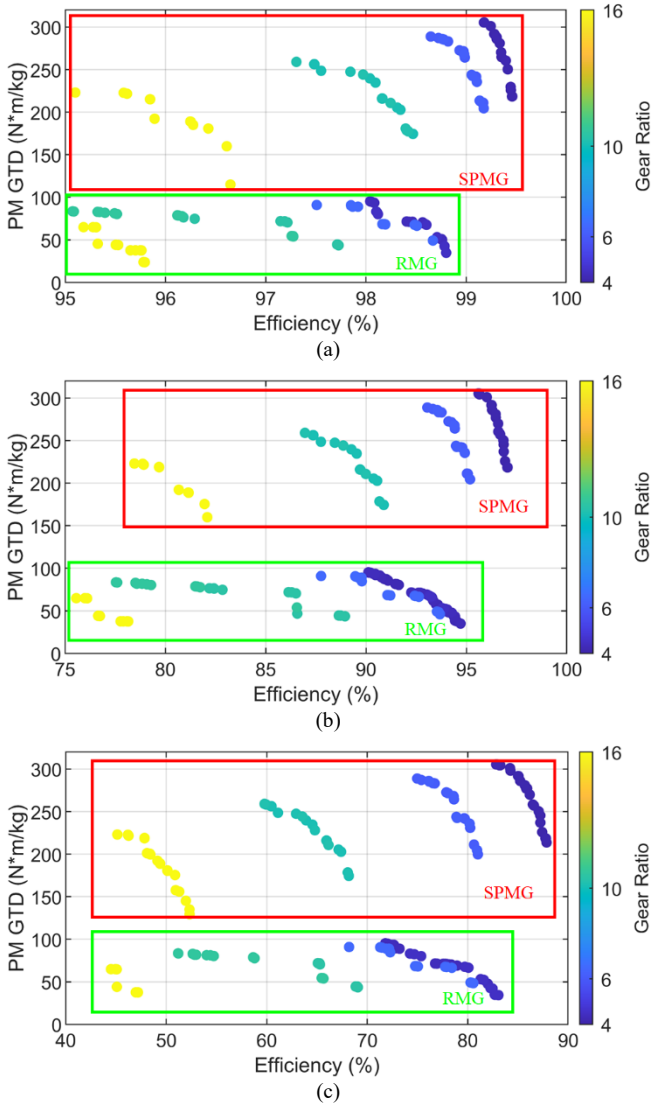

Fig. 5. Pareto optimal fronts maximizing PM GTD and full load electromagnetic efficiency at Rotor 3 speeds of (a) 100 rpm and (b) 1000 rpm (c) 5000 rpm for RMGs and SPMGs with different gear ratios based on 2-D simulations.

Fig. 6 shows how the losses in both topologies correspond to the change of Rotor 3 speed in the most efficient designs that were simulated. The loss per unit parameter has been defined as the ratio of the losses to the output power. As the speed increases, both gears experience higher losses, but the loss distribution is different. While the presence of the Rotor 1 PMs in SPMGs does result in an additional source of losses, the overall efficiencies of the SPMGs are higher than those of the

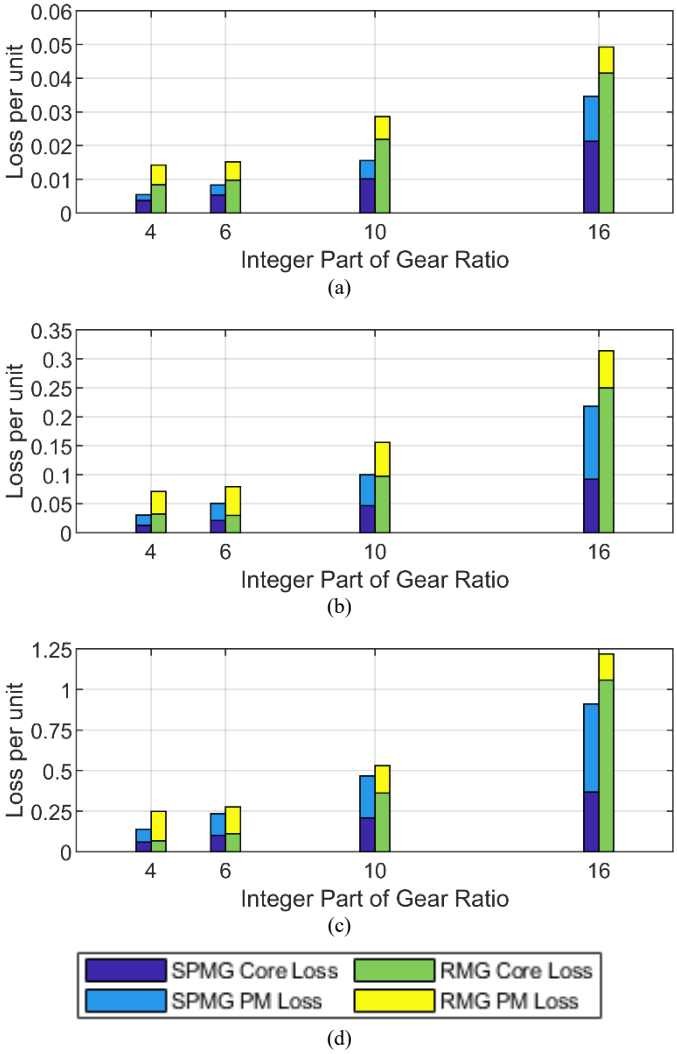

Fig. 6. Corresponding loss amplitude for the designs with maximum efficiency at Rotor 3 speeds of (a) 100 rpm, (b) 1000 rpm, and (c) 5000 rpm, for RMGs and SPMGs with different gear ratios, based on 2-D simulations.

RMGs because the SPMGs can produce significantly more torque with the same amount of active material.

The PMs experience eddy current losses, which increase quadratically with the speed. The core losses in the back irons, modulators, and Rotor 1 teeth have two components, eddy current losses and hysteresis losses, which are proportional to the square of the frequency and to the frequency itself, respectively. Since the RMG has no Rotor 1 PMs, the most efficient RMG design experiences a lower percentage of its losses as PM losses than the optimal SPMG design. However, the RMG tends to suffer significantly larger per unit core losses because it requires significantly more core material to produce the same torque as an SPMG. Thus, even at a Rotor 3 speed of 5000 rpm, the most efficient RMG is still less efficient than the most efficient SPMG.

While [11] compares two nonoptimized designs and concludes that the torque ripple in the RMG is higher than it is in the SPMG, the choice of an integer gear ratio results in very large torque ripples, which may not be representative of designs with non-integer gear ratios. To determine whether this is the case for optimized designs, the torque ripple is evaluated for the RMG and SPMG designs with the maximum VTD or PM GTD for $G_{Int} = 4$, using 2-D FEA. Rotor 2 is fixed, and Rotors 1 and 3 are rotated at the maximum torque orientation according to the gear ratio. Fig. 7 shows the torque on both rotors and reveals that the torque ripple on Rotor 1 tends to be much larger than the torque ripple on Rotor 3, even though the average torque on Rotor 1 is much lower than the average Rotor 3 torque, as found in [18]. Additionally, the optimal RMG designs have much more significant torque ripples than the optimal SPMG designs.

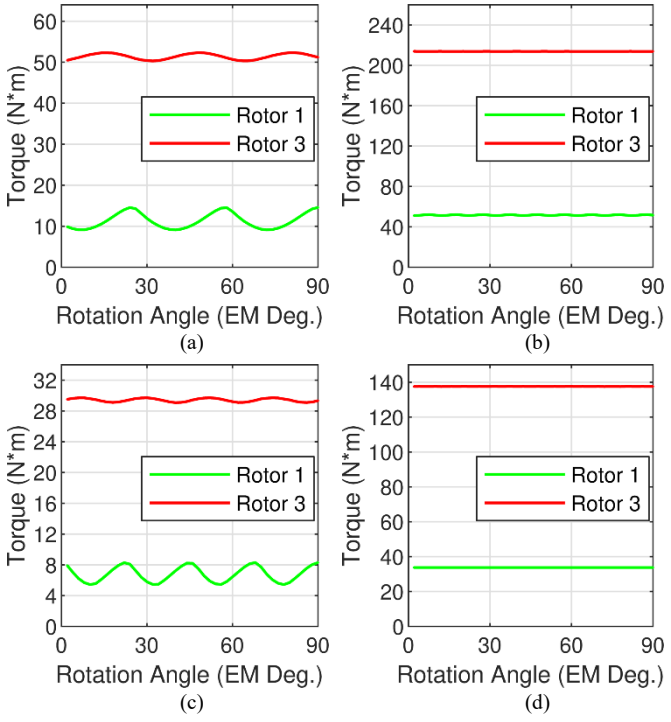

Fig. 7. Rotor 1 and Rotor 3 torque ripple characteristic for continuous operation at the maximum torque orientation of (a) the RMG with maximum VTD, (b) the SPMG with maximum VTD, (c) the RMG with maximum PM GTD, and (d) the SPMG with maximum PM GTD based on 2-D simulations.

Fig. 8 illustrates the corresponding torque ripple percentages for the RMG and SPMG designs with the maximum PM GTD in Fig. 4. The torque ripple percentage is defined as the ratio of the peak-to-peak torque ripple of each rotor to its average torque. For both topologies, the torque ripple tends to decrease as the number of Rotor 1 pole pairs or teeth increases. In a

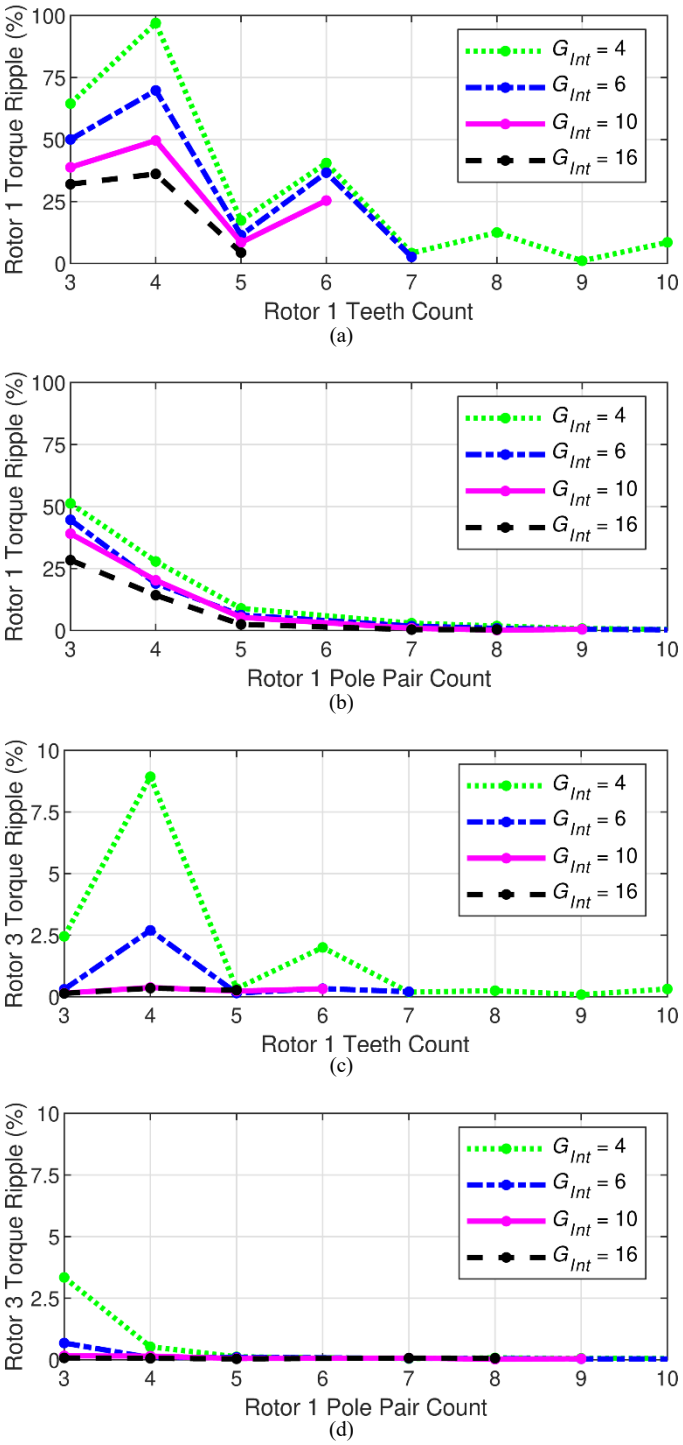

Fig. 8. Corresponding Rotor 1 torque ripple percentages for the (a) RMG and (b) SPMG designs with maximum PM GTD and corresponding Rotor 3 torque ripple percentages for the same (c) RMG and (d) SPMG designs based on 2-D simulations.

design with a fixed gear ratio, as the Rotor 1 pole count or teeth count increases, Q_2 and P_3 will also increase, so there will be lower torque ripple percentages due to the higher values of the least common multiple (LCM) of the pole counts of the two rotating rotors [3]. Thus, one reason that the RMG designs of Fig. 7 have higher torque ripples than the SPMG designs is that the optimal RMG Rotor 1 tooth counts tend to be lower than the optimal SPMG Rotor 1 pole pair counts.

In Figs. 8(a) and 8(c), the RMG designs with even Rotor 1 tooth counts exhibit significantly larger torque ripples than the designs with odd tooth counts. Based on (15) and (22), these designs with even Rotor 1 tooth counts have symmetry, while the designs with odd tooth counts do not have symmetry. Designs with symmetry tend to experience larger torque ripple percentages [3]. For both topologies, lower gear ratios tend to produce higher torque ripple percentages for a fixed Rotor 1 tooth count or pole count due to the lower LCM of the pole counts [3]. As the gear ratio or the pole counts increase, both topologies tend to exhibit very small torque ripples.

Comparing Figs. 8(c) and 8(d) with Figs. 8(a) and 8(b) reveals that, for both topologies at any gear ratio, Rotor 3 exhibits a much smaller torque ripple percentage than Rotor 1 because of higher pole counts and larger average torques. In both topologies, the Rotor 3 torque ripple percentage becomes negligible as the gear ratio or Rotor 1 teeth or pole count is increased.

The opposing sets of magnets facing each other in SPMGs produce significant axially escaping flux, which reduces the torque [21]. Thus, since RMGs only have a single set of PMs, RMGs might experience less of a reduction in torque than SPMGs when simulated in 3-D. To investigate this hypothesis, a subset of the designs with maximum PM GTD and minimum torque ripple for both topologies were simulated as 3-D models. The stack length was varied from 20 to 70 mm, according to Table I. Fig. 9 shows the designs with maximum PM GTD and their corresponding ratio of 3-D torque over 2-D torque for different gear ratios and stack lengths. Figs. 9(a) and 9(b) indicate that higher PM GTD is obtained in designs with lower gear ratios. Comparing Figs. 9(c) and 9(d) disproves the hypothesis that the RMGs may suffer significantly less end effects than SPMGs with the same gear ratios and stack lengths. For the designs with a stack length of 20 mm, the RMG torque predicted by the 3-D model is less than 75% of the 2-D model prediction, while most of the SPMGs experience less than a 20% reduction when the 3-D model is used. The optimal RMG design for any gear ratio has fewer Rotor 3 pole pairs than the optimal SPMG design. The lower the pole count, the further the flux must travel to close its path, which results in more torque reduction in 3-D. However, due to the RMGs' lower VTDs, they may require longer stack lengths than SPMGs to achieve a target torque for a fixed outer diameter; in this case, the longer stack length required by an RMG would make its end effects less significant.

Figs. 3 and 4 also indicate that the RMG experiences a slightly smaller reduction in performance than the SPMG as the gear ratio increases, at least in the range where the optimal RMG Rotor 1 teeth count was simulated. Thus, especially at large radii, the RMG might become a more reasonable option for

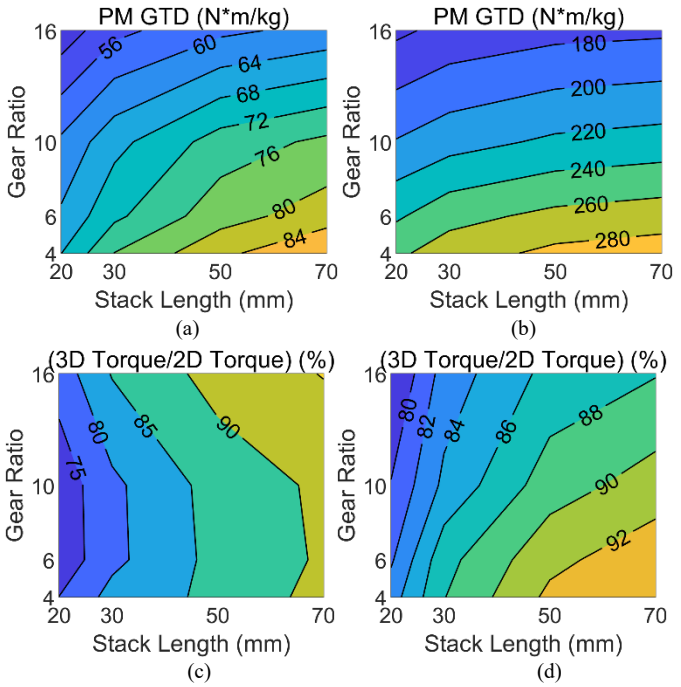

Fig. 9. Variation of the maximum achievable PM GTD based on 3-D simulations for (a) RMGs and (b) SPMGs and the corresponding ratio of 3-D simulation torque to 2-D simulation torque for these (c) RMGs and (d) SPMGs.

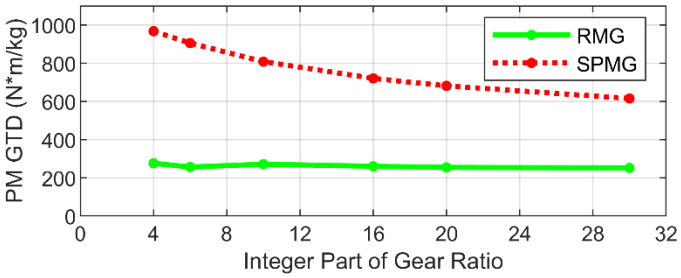

Fig. 10. Impact of gear ratio on PM GTD at a 300mm outer radius based on 2-D simulations.

situations requiring a very large gear ratio in a single stage. Therefore, to obtain the results shown in Fig. 10, the gear ratio of 30 was added and the outer radius was increased to 300 mm. Fig. 10 shows that the RMG's PM GTD varies less with gear ratio than the SPMG's PM GTD. As the integer portion of the gear ratio increases from 4 to 30, the achievable PM GTD decreases by approximately 8% for the RMG and 36% for the SPMG. The semi-constant performance of RMGs for any gear ratio might be interesting for specific applications. However, even at the gear ratio of approximately 30, the SPMG can still achieve significantly higher torque densities than the RMG.

V. Conclusion

This study analyzes and evaluates the performance of a magnetic gear topology previously proposed for high-speed applications. The RMG topology replaces the magnets on the high-speed rotor with a reluctance structure. The operating principle of an RMG is similar to that of an SPMG, and its governing equations are derived in this paper. The performance capabilities of the RMG and SPMG topologies are compared.

An extensive parametric evaluation was used to independently optimize the RMG and SPMG topologies for maximum VTD, PM GTD, and GTD based on 2-D and 3-D FEA simulations. It is shown that the magnet utilization of an optimized RMG is significantly less than that of an optimized SPMG, so the RMG may use on the order of 3 times as much magnet material to achieve a target torque. Also, due to its low torque density, an RMG may require about 5 times as much active volume as an SPMG to achieve the same torque. Furthermore, the efficiency comparison for the optimal designs of both topologies shows that the SPMGs outperform the RMGs across a wide range of speeds. The magnet utilization and efficiency results disagree with the proposed benefits of RMGs for high speeds touted based on comparisons of nonoptimized designs in other papers. The RMGs remove a set of magnets, but their inability to achieve a comparable torque density to SPMGs makes them require thicker magnets or a longer stack length. The transient simulations show that removing the magnets from the high-speed rotor does not improve the efficiency because the RMGs require more core material to provide a desired torque.

Additionally, the torque ripples of both structures are shown for the optimal VTD and PM GTD designs. The optimal RMG designs tend to have lower Rotor 1 teeth counts compared to the Rotor 1 pole counts of the optimal SPMGs. Thus, the RMGs have fewer poles on Rotor 3, which reduces the LCM of the pole counts and produces higher torque ripples on the rotors. Additionally, the lower pole counts of RMGs produces longer flux paths. Thus, even though RMGs lack the opposing sets of magnets, which produce axially escaping flux, RMGs suffer comparable torque reductions from end effects as SPMGs with similar diameters and stack lengths.

Simulations also revealed that the torque densities of RMGs vary less with gear ratio than those of SPMGs. Nonetheless, even at a gear ratio of 30 and a large outer radius, SPMGs were still able to achieve a better magnet utilization than RMGs.

Based on the results, it is evident that the SPMG topology can outperform the RMG topology in terms of torque density, efficiency, and torque ripple. Although the SPMG has magnets on the high-speed rotor, which incur eddy current losses and result in potential mechanical challenges at high speeds, the SPMG can provide a target torque in a smaller volume and a lighter mass with a more efficient design, which also uses the magnets more effectively. Thus, RMGs may only be suitable for applications where environmental or mechanical constraints prohibit the use of magnets on the high-speed rotor.

ACKNOWLEDGMENT

Portion of this research were conducted with the advanced computing resources provided by Texas A&M Performance Research Computing.

The authors would like to thank ANSYS for their support of the EMPE lab through the provision of FEA software.

REFERENCES

[1] T. Frandsen, L. Mathe, N. Berg, R. Holm, T. Matzen, P. Rasmussen, and K. Jensen, “Motor integrated permanent magnet gear in a battery electrical vehicle,” *IEEE Trans. Ind. Appl.*, vol. 51, no. 2, pp. 1516–1525, Mar./Apr. 2015.

[2] L. MacNeil, B. Claus, and R. Bachmayer, “Design and evaluation of a magnetically-geared underwater propulsion system for autonomous underwater and surface craft,” in *Proc. Int. Conf. IEEE Oceans*, 2014, pp. 1-8.

[3] N. Frank and H. Toliyat, “Gearing ratios of a magnetic gear for wind turbines,” in *Proc. IEEE Int. Elect. Mach. Drives Conf.*, 2009, pp. 1224–1230.

[4] K. K. Uppalapati, J. Z. Bird, D. Jia, J. Garner, and A. Zhou, “Performance of a magnetic gear using ferrite magnets for low speed ocean power generation,” in *Proc. IEEE Energy Convers. Congr. Expo*., 2012, pp. 3348–3355.

[5] K. Atallah and D. Howe, “A novel high-performance magnetic gear,” *IEEE Trans. Magn*., vol. 37, no. 4, pp. 2844–2846, Jul. 2001.

[6] S. Gerber and R. J. Wang, “Torque capability comparison of two magnetically geared PM machine topologies,” in *Proc. Int. Conf. Ind. Technol*., 2013, pp. 1915-1920.

[7] C. Liu, J. Yu, and C. H. T. Lee, “A New Electric Magnetic-Geared Machine for Electric Unmanned Aerial Vehicles,” *IEEE Trans. Magn*., vol. 53, no. 11, pp. 1-6, Nov. 2017.

[8] Y. Wang, J. Ma, C. Liu, G. Lei, Y. Guo, and J. Zhu, “Reduction of Magnet Eddy Current Loss in PMSM by Using Partial Magnet Segment Method,” *IEEE Trans. Magn*., vol. 55, no. 7, pp. 1-5, Jul. 2019.

[9] L. Li, W. Li, D. Li, X. Zhang, and Y. Fan, “Influence of sleeve thickness and various structures on eddy current losses of rotor parts and temperature field in surface mounted permanent-magnet synchronous motor," *IET Elect. Power Appl.*, vol. 12, no. 8, pp. 1183-1191, Sep. 2018.

[10] F. Chai, Y. Li, P. Liang, and Y. Pei, “Calculation of the Maximum Mechanical Stress on the Rotor of Interior Permanent-Magnet Synchronous Motors,” *IEEE Trans. Ind. Electron.*, vol. 63, no. 6, pp. 3420-3432, Jun. 2016.

[11] K. Aiso, K. Akatsu, and Y. Aoyama, “A Novel Reluctance Magnetic Gear for High-Speed Motor,” *IEEE Trans. Ind. Appl*., vol. 55, no. 3, pp. 2690-2699, May/Jun. 2019.

[12] K. Li, Z. Zhu, and P. Wu, “A Reluctance Magnetic Gear for High Speed and Vibration Motor Systems,” in *Proc. Int. Conf. Mechatronics Mach. Vision Pract.*, 2018, pp. 1-5.

[13] A. F. Shevchenko, A. G. Pristup, G. B. Vyalcev, D. M. Toporkov, and K. T. Alieva, “Electromagnetic Torque of Reluctance Magnetic Gear,” in *Proc. Int. Sci. Tech. Conf. Actual Problems Electron. Instrument Eng.*, 2018, pp. 402-405.

[14] K. Aiso, K. Akatsu, and Y. Aoyama, “A novel magnetic gear for high speed motor system,” in *Proc. IEEE Int. Elect. Mach. Drives Conf.*, 2017, pp. 1-7.

[15] M. S. Arani and S. A. Afsari, “Design of Rotor Structure for Reluctance Magnetic Gear to Improve Torque Characteristic,” in *Proc. Power Electron. Drives Syst. Technol. Conf.*, 2020, pp. 1-5.

[16] M. Johnson, A. Shapoury, P. Boghrat, M. Post and H. A. Toliyat, “Analysis and development of an axial flux magnetic gear” in *Proc. IEEE Energy Convers. Congr. Expo*., 2014, pp. 5893-5900.

[17] M. Johnson, M. C. Gardner, and H. A. Toliyat, “Design comparison of NdFeB and ferrite radial flux surface permanent magnet coaxial magnetic gears,” *IEEE Trans. Ind. Appl.*, vol. 54, no. 2, pp. 1254–1263, Mar./Apr. 2018.

[18] M. Johnson, M. C. Gardner, H. A. Toliyat, S. Englebretson, W. Ouyang, and C. Tschida, “Design, Construction, and Analysis of a Large-Scale Inner Stator Radial Flux Magnetically Geared Generator for Wave Energy Conversion,” *IEEE Trans. Ind. Appl.*, vol. 54, no. 4, pp. 3305-3314, Jul./Aug. 2018.

[19] M. C. Gardner, B. E. Jack, M. Johnson, and H. A. Toliyat, “Comparison of Surface Mounted Permanent Magnet Coaxial Radial Flux Magnetic Gears Independently Optimized for Volume, Cost, and Mass,” *IEEE Trans. Ind. Appl.*, vol. 54, no. 3, pp. 2237-2245, May/Jun. 2018.

[20] K. Aiso, K. Akatsu and Y. Aoyama, "Reluctance magnetic gear and flux switching magnetic gear for high speed motor system," in *Proc. IEEE Energy Convers. Congr. Expo*., 2017, pp. 2445-2452.

[21] S. Gerber and R-J. Wang, “Analysis of the end-effects in magnetic gears and magnetically geared machines,” in *Proc. IEEE Int. Conf. Elect. Mach.*, 2014, pp. 396-402.